Differentiating Pinch and Grasp using sEMG

Brendan P. Beauchamp
Department of Engineering
Grand Valley State University
Grand Rapids, Michigan
beauchab@mail.gvsu.edu

Dr. Samhita Rhodes
Department of Engineering
Grand Valley State University
Grand Rapids, Michigan
rhodesam@gvsu.edu

***Abstract*— This paper applies sEMG enveloping, median frequency, and coherence to the Sollerman Hand Function Test Dataset recorded by Jarque Bou et al in order to differentiate sEMG activity during pinching and grasping tasks. Pinches and Grasps were found to cause very different activation patterns in sEMG spot 3 relating to flexion of digits I - V. Median frequency was found to be less correlated with differentiation and provided information about the degree of object manipulation performed during each task. Coherence was shown to increase between flexors and extensors with intensity of task, some spectral results correlated between finger flexor and extensor power spectra.**

Keywords*— *sEMG, SHFT, MSC, Median Frequency, Forearm, Pinch, Grasp

I. Introduction

Sollerman Hand Function Test (SHFT) surface electromyography (sEMG) and joint angles collected by Jarque Bou et al are analyzed in this experiment for the purpose of differentiating pinch and grasp tasks using only sEMG. This is performed through the application of sEMG enveloping, median frequency analysis, coherence, and observation of fingertip joint angles over time. The differentiation of pinch and grasp tasks in the Jarque Bou dataset using sEMG is significant because all digit flexors are shown to be observable from a single sEMG sensor [6]. This paper investigates the depth of information which can be extracted from this point.

II. Methods

A. Experiment

Gestures within the SHFT were differentiated between pinching and grasping tasks, then sEMG was observed using measures of activation, and median frequency. Joint angles were observed for the ensemble average of the PIP and MCP for digits II-V, and index finger, while the IP, MCP, and CMC are observed for the thumb. Muscle groups observed included thumb, index finger, and ensemble finger flexion and extension. Muscles were not measured directly, but instead through 7 optimal locations for forearm sEMG measurement as described by Jarque Bou [6] and shown below in table 1.

As shown through previous research, many muscles overlap underneath these seven sEMG spots [6,7,10]. The actions associated with sEMG spots in table 1 are correlated to the muscles reported by Jarque Bou to be directly below the electrodes [6]. Only spots 3,4, and 5 constitute bilateral motion in the fingertip workspace, all other recording spots measure wrist motion. Because spot 3 measures all digit flexors, it is used to indicate intensity.

Table 1: sEMG Spot and Associated Action

Spot	Actions
1	Wrist Flexion & Ulnar Deviation
2	Wrist Flexion & Radial Deviation
3	Flexion I-V
4	Extension I
5	Extension II-V
6	Wrist Extension and Ulnar Deviation
7	Wrist Pronation, Supination, Extension

B. Data Collection and Filtering

The dataset used in this study was designed by Jarque-Bou et all and observes the Sollerman Hand Function test through seven sEMG signals representative of all muscle activity in the forearm and fingertip joint angles recorded by the Cyberglove 1[6]. This dataset was designed to aid in physiologic study of the forearm, and is notable for its investigation into optimal sEMG recording and integration with the fingertip workspace in 16 degrees of freedom (DOF). SX230 electrodes were used in conjunction with an sEMG Biometrics Ltd device to collect the data with a gain of 1000. Data was sampled at a frequency of 1 kHz and has a usable bandwidth between 20 and 460 Hz. Joint and envelopes by Jarque Bou were resampled to 100 Hz. Patients' hair was removed by shaving and skin was cleaned with alcohol before the electrodes were placed. Signal filtering was performed using a fourth order band pass filter between 25 and 500 Hz on raw sEMG [6].

C. Enveloping and Activation

In order to observe the activation of muscles, two different enveloping functions were observed. The first is from the Jarque Bou Dataset itself, raw sEMG is rectified and filtered using a fourth order low pass filter at 8 Hz and gaussian smoothing [6]. Furthermore, activation analogous to Hill Type Muscle activation is investigated in this research by rectifying and filtering using a 4th order butterworth lowpass filter at 4 Hz [8]. Application of the second order recursive filter is not performed due to lack of knowledge on electromechanical delay and scaling coefficients for musculoskeletal models of the forearm [8].

While the rectified and filtered envelope is reported by Heine et al to be a poor representation of neural drive, this assessment pertains to the nonlinearities of the peaks of the envelope [8]. The application of the filter is instead used for comparison to the enveloped sEMG within the dataset.

D. Median Frequency Analysis

Median frequency was observed to track changes in frequency spectra of flexor sEMG with tasks of varying intensity flexion. This was done without any window overlap. The algorithm is shown below in equations 1 and 2 where total power is first calculated for each time segment (1), then power summation is reiterated until the half power point is reached (2). Median Frequency is commonly used in sEMG studies as an indicator for fatigue, and has also been shown by Thopanja et al to be an indicator for joint angle motion [2,4]. The median frequency vector is then regressed for the timespan in which the subject is touching the object under manipulation in order to observe frequency changes based on the specific ADL. Furthermore, this reduction of time span removes the effect of resting frequency of the muscles from the regression.

$$P_{tot} = \sum_{f=0}^{f_{max}} X^2(f) \quad (1)$$

$$\sum_{f=0}^{f_M} X^2(f) = \frac{1}{2} P_{tot} \quad (2)$$

D. Magnitude Squared Coherence Analysis

Magnitude-squared coherence (MSC) is a frequency domain analog of a squared correlation coefficient (r2), the work of Lovett et al develops a Coherence Spectrogram (CS) which can be used to observe localized changes in coherence between two signals [3]. The algorithm involves calculating the average of a DPSS sequence windowed MSC for every second in the signal. The CS can be interpreted as the cross spectra divided by the spectrograms of the two signals. The equations for the CS and spectrogram are shown respectively in equations 3 and 4.

$$CS[n,k] = \frac{\left|\sum_{i=0}^{L-1} X_i[n,k] Y_i^*[n,k]\right|^2}{\sum_{i=0}^{L-1} \left|X_i[n,k]\right|^2 \sum_{i=0}^{L-1} \left|Y_i[n,k]\right|^2} \quad (3)$$

$$S[n,k] = \sum_{i=0}^{L-1} \left|X_i[n,k]\right|^2 \quad (4)$$

III. Results

Shown below in figure 1 is a box chart displaying the intensity of flexor activity for all 26 ADL. Of particular interest to this investigation were ADL 1,3, 6 and 14 in which the intensity of flexion was varied controllably. In ADL 1 and 3, subjects are picking up coins on a desk, putting them in a purse, and retrieving them from the purse respectively. ADL 6 involves picking up a screwdriver, and turning a screw 360 degrees with it, while ADL 14 increases flexion force further by cutting a cold cake with a knife.

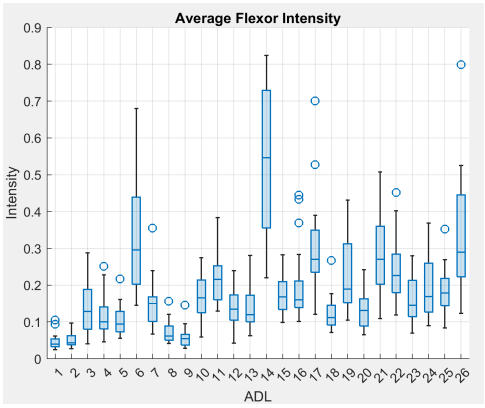

Figure 1: Intensity of all ADL Spot 3 (Digit I-V Flexion)

A. Pinch and Grasp Excitation

Figure 2 displays the activation envelope reported by Jarque Bou et al and the envelopes derived using the filtering reported by Heine. As shown, the Heine envelope appears to match the shape of the Bou envelope, but the Bou envelope has had gaussian smoothing applied to it. Due to the similarity seen between the two envelopes, the envelope applied by Jarque Bou is used to observe joint angles in further investigation for this experiment.

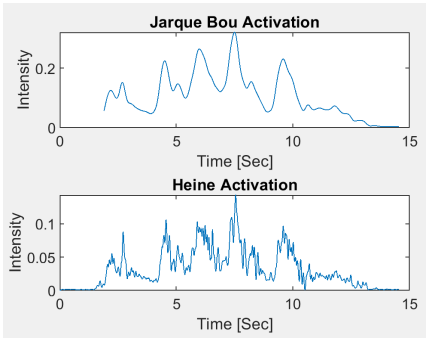

Figure 2: Bou and Heine Envelope Comparison

Four tasks were found to be representative of the gradient between a pinch and a grasp, namely; ADL 1, 3, 6, and 14. Activation envelopes for digits I - V flexion, digits II-V extension and digit I extension were observed with cyberglove joint angles for digit I, digit II, and an ensemble of digits II-V. Red asterisk bound the time a subject has an object under manipulation.

Shown below in figure 3 are the MCP and PIP for digit I, digit II, and an ensemble average of digits II - V along with the activation envelopes for digits I-V flexion, digits II-V extension, and digit I extension for ADL 1. ADL 1 involved collecting a coin and putting it into a change purse. Observing the activation envelope for digit I flexion, it is noted that there is two pulses which occur before the subject grasps the coin, and that there is a decrease in intensity of all fingertip workspace actuators from the point the coin is touched to the point that it is placed in the purse. There are similar pulses observed in both digit I extension and digit II extension.

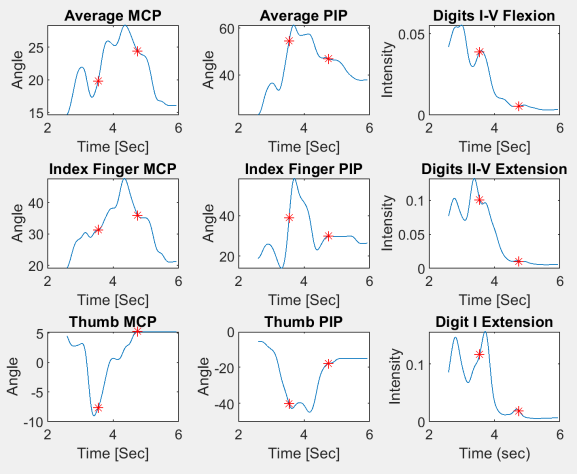

Figure 3: Subject 1 ADL 1 (Pulp Pinch)

Figure 4 displays the same parameters in the hand model as those in figure 3, but for ADL 3. ADL 3 involves removing the coin placed within the coin purse, and leaving it on the table. It is noted that there is much higher intensity sEMG observed in this experiment, and that there are several pulses of flexor intensity while the subject is holding on to the coin. It is further noted that in this experiment, digit II-V extension becomes tetanized with high intensity. There is much more volatility in the joint angle motion for this ADL.

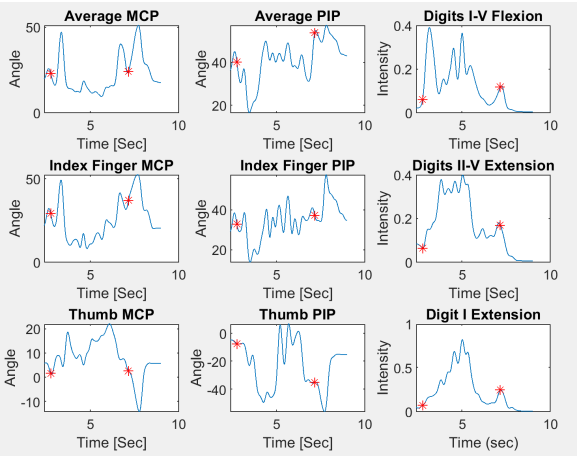

Figure 4: Subject 1 ADL 3 (Pulp Pinch)

Shown below in figure 5 are similar joint angle and intensity data to previous experiments for ADL 6. ADL 6 involves taking a screwdriver and turning a screw 360 degrees with it. All sEMG appear to tetanize in this experiment, and joint angles fluctuate rapidly. Notably, four pulses appear in the stimulation of the three observed sEMG spots. Observing the average PIP and digit II PIP, these pulses are visible as quick fluctuations in joint angle as the subject twists the screwdriver. Intensity of sEMG does not settle to zero in between pulses, suggesting that force is used to oppose the pulses generated in antagonistic muscles.

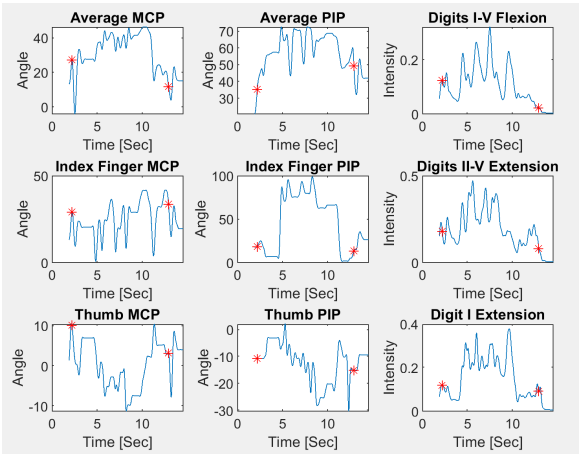

Figure 5: Subject 2 ADL 6 (Diagonal Volar Grip)

Shown below in figure 6 are the markers for fingertip workspace and sEMG intensity for ADL 14. ADL 14 involves taking a knife with the right hand and a fork with the left hand to split a piece of clay while sitting. This ADL involves significant force and control of the knife, this control is reflected in the frequency and amplitude of stimulus observed in sEMG intensity. Joint angles are held nearly constant with minor fluctuations for stabilization and adjustment of grip.

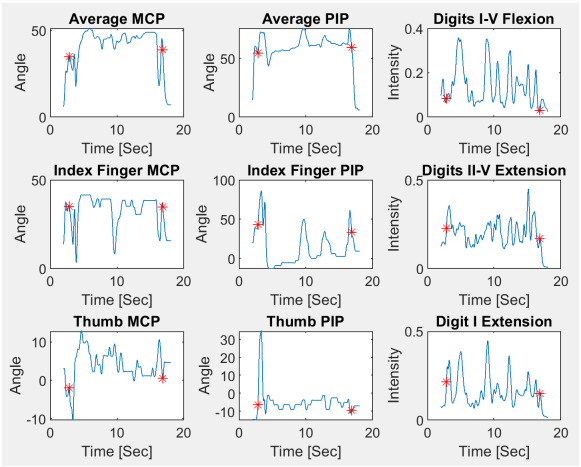

Figure 6: Subject 1 ADL 14 (Diagonal Volar Grip)

B. *Frequency Analysis*

Shown below in figure 7 is the median frequency of flexors for digits I-V during ADL 1 with time the subject is manipulating a coin linearly regressed. Median frequency while the coin is being held is roughly 70 Hz, but fluctuates more right before the coin is released. Interestingly, the median frequency decreases before the hand touches the coin. Before the hand is used for manipulation, much higher and more volatile median frequencies appear.

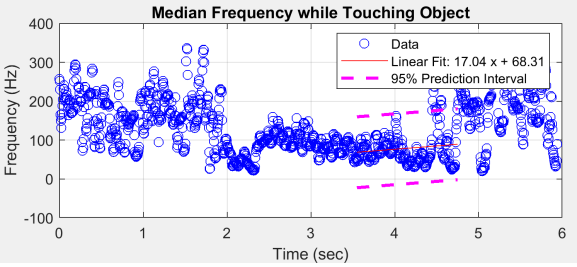

Figure 7: Subject 1 ADL 1 Median Frequency

Shown below in figure 8 is the power spectra observed for flexors in ADL 1. Comparing figures 7 and 8, it is seen that the high median frequency at the beginning and end of the trial was not caused by a high power signal. In contrast, a high intensity low frequency signal can be seen where the median frequency drops. This high intensity patch is also related to an increase in flexor activation in the time domain.

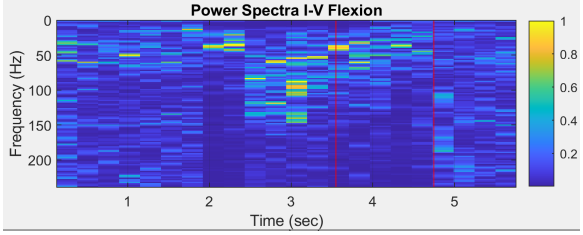

Figure 8: Subject 1 ADL 1 Spectrogram

Shown below in figure 9 is the median frequency for flexors during ADL 3 similarly to ADL 1 above. In the time domain, ADL 3 exhibited tetanization which was not seen in ADL 1. In the frequency domain this translates to significantly more motor unit activation sustained over time. The median frequency in figure 9 is regressed with a much greater y intercept frequency, and has a negative slope instead of a positive one as shown in ADL 1. Furthermore contrasting the pinch observed in ADL 1 and ADL 3 is that the coin was manipulated for much longer in ADL 3. There is less time where the fingers are manipulated before the object is grasped in ADL 3.

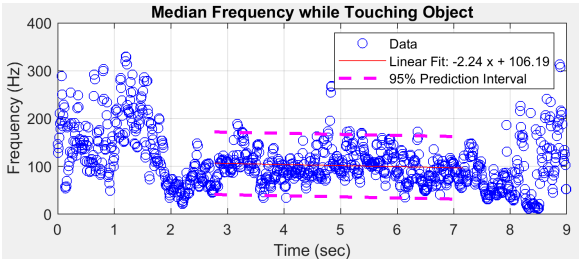

Figure 9: Subject 1 ADL 3 Median Frequency

Figure 10 displays the spectrogram for flexor sEMG during ADL 3. There is significantly more spectral activity observed in ADL 3 than there is in ADL 1. Comparing the time domain activation for the two pinches, it can be seen that the larger amount of spectral activity relates to the tetanization of the pinch flexion in ADL 3. The highest intensity spectral activity seems to occupy the same range in both ADL. The beginning and end of flexor activation exhibit a decrease in frequency.

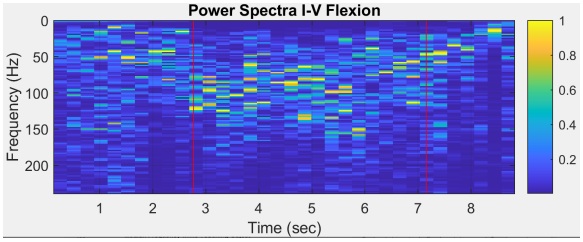

Figure 10: Subject 1 ADL 3 Spectrogram

Shown below in figure 11 is the median frequency for flexor sEMG in ADL 6. Similar to ADL 3, the object is manipulated for much longer than ADL 1. Interestingly though, the median frequency of ADL 6 is between the median frequencies of ADL 1 and 3 despite generating larger activation envelopes than both of them in the time domain. While flexor activation intensity was greater for flexors in ADL 6 than in ADL 3, Jarque Bou reported an overall greater activation of sEMG in ADL 6 than 3. Furthermore, Jarque Bou reported a greater degree of joint angle manipulation in ADL 6 than in ADL 3.

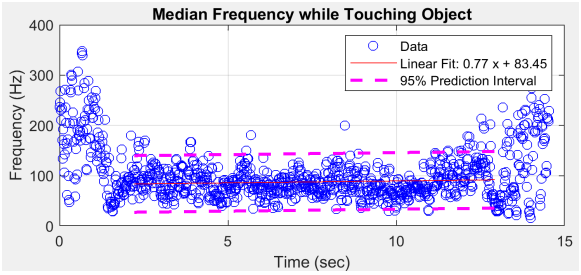

Figure 11: Subject 2 ADL 6 Median Frequency

Figure 12 shows the spectrogram for flexor sEMG during ALD 6. This experiment appears to show further tetanization than that observed in ADL 3, and continues for a longer duration. When observing the spectrogram, it is not initially clear that the median frequency is lower in ADL 6 than it is in ADL 3. Furthermore, the intensity of contraction is also abstracted from the spectrogram.

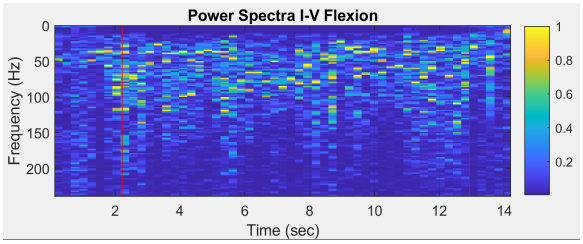

Figure 12: Subject 1 ADL 6 Spectrogram

Shown in figure 13 is the median frequency of flexor sEMG during ADL 14. The median frequency observed in ADL 14 is the largest observed in the dataset. It is the second largest decrease in median frequency during object manipulation, with ADL3 causing the largest decrease. This is interesting because Jarque Bou reported the largest change in joint angle manipulation from ADL 14, ADL 3 had a comparable change in joint angle manipulation to ADL 1.

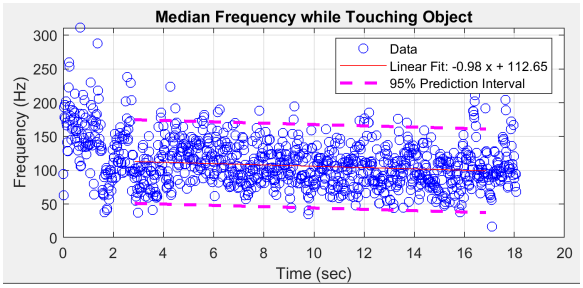

Figure 13: Subject 1 ADL 14 Median Frequency

Shown below in figure 14 is the spectrogram for flexor sEMG during ADL 14. Flexors exhibited the highest amount of activation in ADL 14, and this can be seen below by the high intensity frequency activity between 20 and 150 Hz. ADL 14 also differs from others in that it causes high intensity signals up to nearly 200 Hz. All other ADL stopped near 150 Hz. The background noise of this ADL is significantly higher than other ADL.

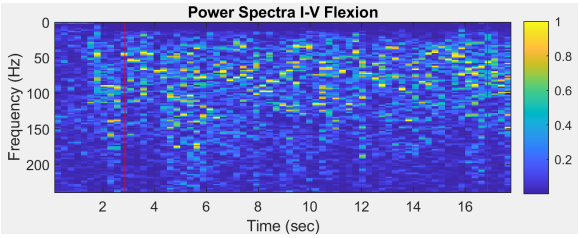

Figure 14: Subject 1 ADL 14 Spectrogram

C. *Coherence Analysis*

Coherence between flexors and extensors of digits II -V are compared with spectral images, activation of muscles, and the average joint angle motion of digits II-V MCP. Coherence was observed to increase from the lightest pinch to the strongest grasp observed. Some Alpha and Gamma wave coherence observed overlapped with power spectra of flexor and extensor sEMG. Coherence appears often when a joint angle must be maintained against an opposing force.

Anticipatory activation appears to be visible in the coherence spectra of flexors and extensors. High coherence is observed in delta through gamma frequencies before the object under manipulation is grasped and let go. This is reflected with power observed near these points, but it does not occupy the same bandwidth as the entire coherence spike. Coherent results present similar bandwidths in spectra and the coherence may be caused by sEMG sensors measuring the same source.

Shown below in figure 15 are the power spectra, intensity time plots and coherence for digits I-V flexion and digits II-V extension during ADL1. Low frequency coherence in delta - alpha band appears near chirps in the spectra of flexion and extension. Coherent spikes in the beta and delta range also correlate with high power information in the spectrograms. The patch of delta coherence near 60 Hz and 5 seconds also shows up in both of the power spectra at low intensity. A decreasing chirp in beta-gamma coherence is present during the largest change in joint angles, but does not appear to relate to high power spectra of flexion or extension.

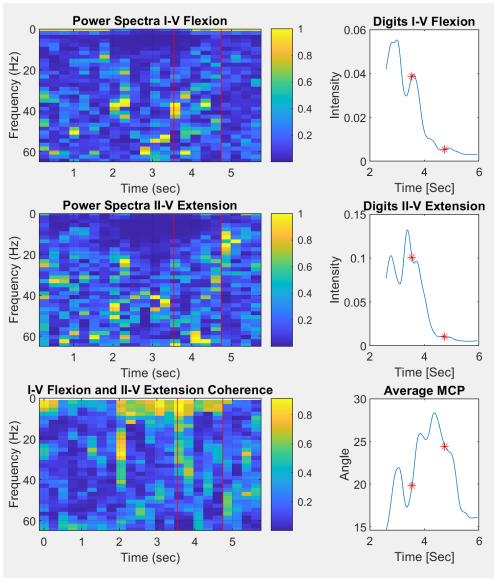

Figure 15: Subject 1 ADL 1 Coherence

Shown below in figure 16 are the power spectra, intensity time plots and coherence for digits I-V flexion and digits II-V extension during ADL 3. Notably despite not relating to high intensity artifacts in either power spectra, beta coherence is much more present in low frequency coherence between the signals. Coherence around 2 seconds and 40 hz appears to relate to power spectra of flexors and extensors, and relates to the start of tetanization of hand muscles. During extension tetanus there is high power visible for extensors, and low power for flexors, this matches their respective intensity graphs. This region correlated to no coherence and a significant change in joint angle. Coherence exhibited after this patch appears to correlate with a high degree of joint angle variance. When both flexors and extensors are at their maximum tetanization, there is no coherence visible from 0-60 Hz.

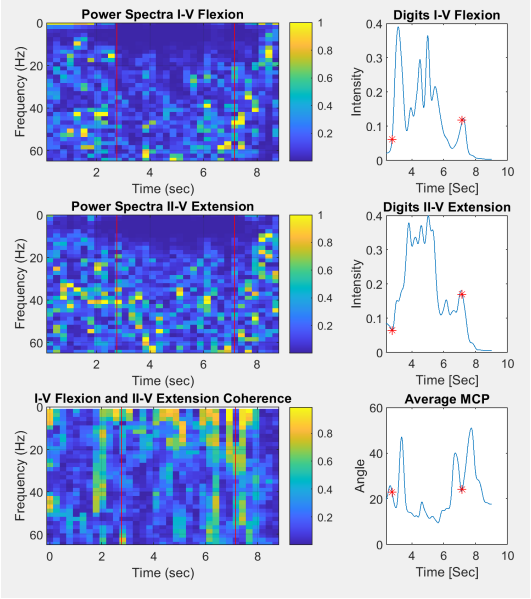

Figure 16: Subject 1 ADL 3 Coherence

Shown in figure 17 are the power spectra, intensity time plots and coherence for digits I-V flexion and digits II-V extension during ADL 6. Similar to all other ADL, there appears to be high coherence in all bandwidths when the user first grasps and lets go of the object being manipulated. This coherence occurs as spikes before the subject grasps and lets go of the object. More coherence in the range of 0.6 to 0.4 is visible in this task than in the pinching tasks. The patch of coherence at 8 seconds near 40 Hz occurs at the same time as a significant decrease in joint angle. Leading up to this point there is an increase in flexor activity and afterward flexors decrease and extensors increase.

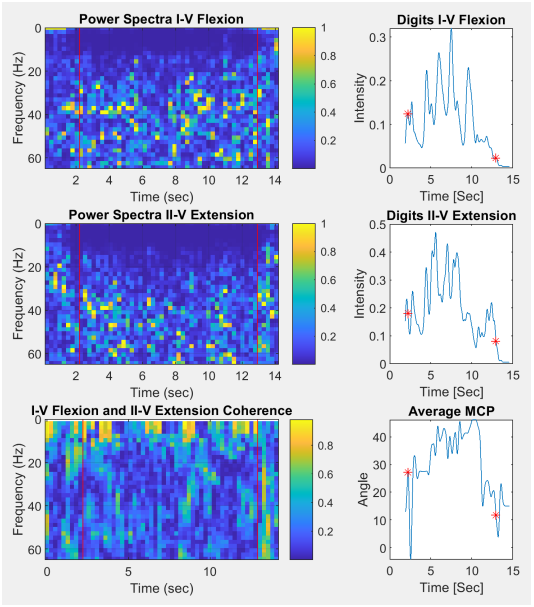

Figure 17: Subject 2 ADL 6 Coherence

Shown below in figure 18 are the power spectra, intensity time plots and coherence for digits I-V flexion and digits II-V extension during ADL 14. ADL 14 exhibits the highest degree of coherence between all datasets, and has an overlapping bandwidth with the power spectra of both flexor and extensor sEMG in alpha and gamma range. Patches of high intensity power occur near patches of high coherence in both flexor and extensor spectra. Furthermore, the MCP angle is held between 40 and 50 degrees suggesting that the hand is making fine adjustments as the knife is used.

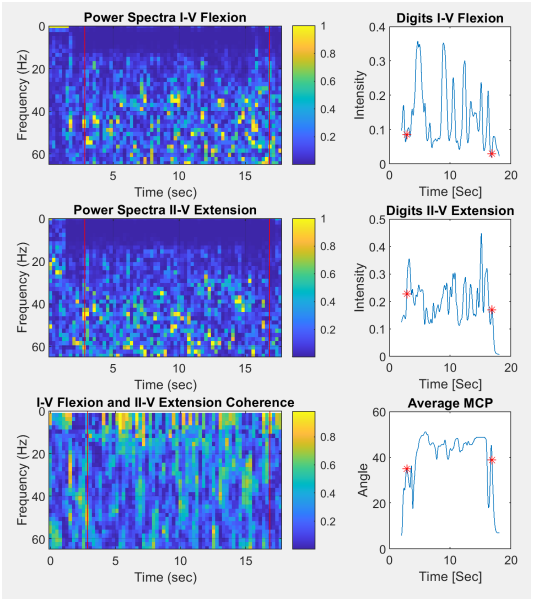

Figure 18: Subject 1 ADL 14 Coherence

IV. Discussion

Results in this research show that pinch and grasp can be easily differentiated through observation of activation intensity of sEMG spot 3. This spot is above the flexor digitorum muscles, which are thought to be the largest contributors to sEMG signal in spot 3. In pinching tasks, the activation was a twitch or light tetanization. Interestingly, the light grasp in ADL 6 led to a smaller initial activation twitch than the grasp in ADL 3. This may be due to the subject digging around a coin purse and needing to coherently grasp a small coin, while in ADL 6 flexion force is used to hold the screwdriver. Supination and pronation are used for rotational force to drive the action of screwing the screw into the board. When flexing to stabilize opposing forces, intensity of activation increases significantly such as observed in ADL 14.

Median frequency was not as useful of a measure for differentiation between pinch and grasp. ADL 1 had the lowest median frequency and ADL 14 had the highest, but ADL 3 had a higher median frequency than ADL 6. This was likely caused by the high degree of flexor manipulation needed to dig around the purse to find the coin, and less related to the intensity of the action. Median frequency was therefore interpreted more as a measure for fine motor control than activation in hand muscles.

Coherence results were subdivided into three categories; one source measured from multiple electrodes, mutual innervation, and anticipatory activation. Low intensity coherence observed in ADL 1 was likely an example of mutual source measurement, and the spikes before and after an object are likely anticipatory activation. This would mean that the opposing muscles coherence is common neural input that the hand is to be manipulated. As forces increase in the ADL, coherence between spots is more likely to be observed, and this coherence is likely either anticipatory or mutual innervation. Low frequency coherence is likely caused by phase alignment of filtered signals at low frequencies.

Implications for further research suggest a similar amount of activation variability in each sEMG spot. Through observation of all spot activations and fingertip workspace data, many more gestures may be differentiable as proposed in conjunctive research [7]. While this dataset does not differentiate individual fingers, it is shown that through measurement of available flexor activation that several degrees of pinch and grasping tasks can be observed. Pinches were observed as twitches and short tetanus, while grasps were observed as continuous tetanus.

V. Conclusion

This paper demonstrates the differentiability of pinch and grasp tasks using the Jarque Bou dataset. The breadth of information on the fingertip workspace included in the Jarque Bou dataset allows researchers to study the hand with a high level of physiologic detail, without the need for direct interaction with subjects or complex recording instruments. Pinches and Grasps were differentiated using activation, light pinches and hard grasps were clearly differentiable actions through the measurement of activation.

References

[1] M. D. F. Ma'as, Masitoh, A. Z. U. Azmi and Suprijanto, "Real-time muscle fatigue monitoring based on median frequency of electromyography signal," 2017 5th International Conference on Instrumentation, Control, and Automation (ICA), 2017, pp. 135-139, doi: 10.1109/ICA.2017.8068428.

[2] S. Thongpanja, A. Phinyomark, C. Limsakul, and P. Phukpattaranont, “Application of mean and median frequency methods for identification of human joint angles using EMG Signal,” *Lecture Notes in Electrical Engineering*, pp. 689–696, 2015.

[3] E. G. Lovett and K. M. Ropella, “Time-frequency coherence analysis of atrial fibrillation termination during Procainamide administration,” *Annals of Biomedical Engineering*, vol. 25, no. 6, pp. 975–984, 1997.

[4] “Biering-Sørensen Test,” *Shirley Ryan AbilityLab*. [Online]. Available: https://www.sralab.org/rehabilitation-measures/beiring-sorensen-test. [Accessed: 15-Nov-2021].

[5] P. A. Ortega-Auriol, T. F. Besier, W. D. Byblow, and A. J. McMorland, “Fatigue influences the recruitment, but not structure, of muscle synergies,” *Frontiers in Human Neuroscience*, vol. 12, 2018.

[6] Jarque-Bou, N. J., Vergara, M., Sancho-Bru, J. L., Gracia-Ibáñez, V., & Roda-Sales, A. (2019). A calibrated database of kinematics and EMG of the forearm and hand during activities of daily living. Scientific Data, 6(1). https://doi.org/10.1038/s41597-019-0285-1

[7] Beauchamp, B. P. (2022). Viable Gestures for Fingertip Workspace HID. *Unpublished*.

[8] Heine, R., Manal, K., & Buchanan, T. S. (2003). Using hill-type muscle models and EMG data in a forward dynamic analysis of joint moment. *Journal of Mechanics in Medicine and Biology*, *03*(02), 169–186. https://doi.org/10.1142/s0219519403000727

[9] R. Merletti and D. Farina, Surface Electromyography: Physiology, Engineering, and Applications. John Wiley & Sons, 2016.

[10] Jarque-Bou, N., Vergara, M., Sancho-Bru, J., Roda-Sales, A., & Garcia-Ibanez, V. (2018, October 29). *Identification of forearm skin zones with similar muscle activation patterns during activities of daily living - journal of Neuroengineering and Rehabilitation*. BioMed Central. Retrieved December 6, 2022, from https://jneuroengrehab.biomedcentral.com/articles/10.1186/s12984-018-0437-0